1,3-Diketone Fluids and Their Complexes with Iron

ARTICLE *in* THE JOURNAL OF PHYSICAL CHEMISTRY A · MARCH 2013

Impact Factor: 2.69 · DOI: 10.1021/jp400980y · Source: PubMed

THE JOURNAL OF PHYSICAL CHEMISTRY A

Article

pubs.acs.org/JPCA

1,3-Diketone Fluids and Their Complexes with Iron

Michael Walter,*[,†,‡] Tobias Amann,[‡] Ke Li,[¶] Andreas Kailer,[‡] Jürgen Rühe,[¶] and Michael Moseler[‡]

[†]FMF, Freiburg Materials Research Center, University of Freiburg, Stefan-Meier-Straße 21, 79104 Freiburg, Germany

[‡]IWM, Fraunhofer Institute for Mechanics of Materials, Woehlerstraße 11, 79108 Freiburg, Germany

[¶]IMTEK, Department of Microsystems Engineering, University of Freiburg, Georges-Köhler-Allee 103, D-79110 Freiburg, Germany

Supporting Information

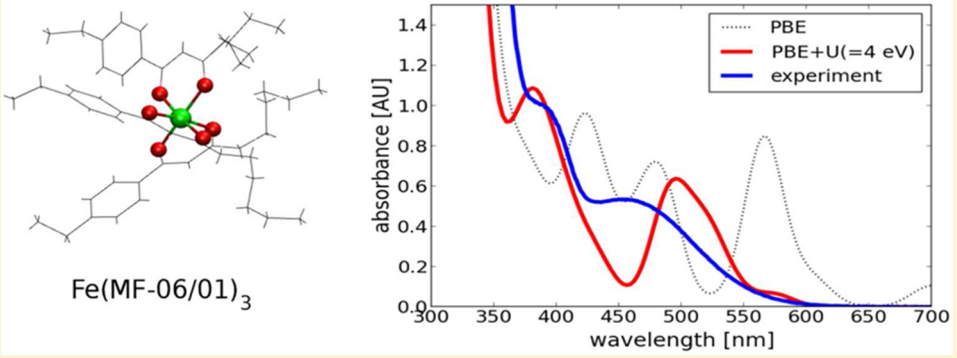

ABSTRACT: Tribological experiments with 1,3-diketone fluids in contact with iron surfaces show ultralow friction, which was suggested to be connected to the formation of iron complexes. In order to support this assumption, we calculate infrared and optical spectra of various substituted 1,3-diketones and their iron complexes using gradient-corrected density functional theory (DFT). The description of the complexes requires the application of the DFT+U scheme for a correct prediction of the high spin state on the central iron atom. With this approach, we obtain excellent agreement between experiment and simulation in infrared and optical spectra, allowing for the determination of 1,3-diketone tautomeric forms. The match in the spectra of the complex strongly supports the assumption of iron complex formation by these lubricants.

INTRODUCTION

Unusual friction properties were observed experimentally by using 1,3-diketone fluids (DKs) as lubricants for iron surfaces.[1−3] In these investigations, the friction coefficient varies with time, and ultralow friction coefficients are reached after some initial running-in period. This period is accompanied by large wear as compared to fully additivated lubricants and by a color change of the lubricant from yellow to red. Intensive red color is well-known from iron complexes,[4] suggesting the formation of a tribochemical complex during the running-in period.[3]

The experimental setup consists of steel surfaces sliding against each other, and the DKs used are phenyl substituted 1,3-diketones. It was suggested that iron is released during friction, and iron is known to form stable complexes with diketones.[5] Both the appearance of a running-in time as well as the large wear indicate that a tribochemical reaction with the surface is crucial for the observed strong reduction of friction. While ultralow friction is not reached by using the complex as the lubricant alone,[1] it is nevertheless likely that complex formation plays an important role in the process.

Here, we report a joint experimental and computational effort to better characterize the tribological experiment and the chemical reactions that are involved. While we briefly describe the experimental methods and results, the main focus of this work is on the simulation. The properties of the DKs and a comparison between experimental and simulated infrared (IR) spectra are discussed. We also report geometrical and electronic structures of the complexes where the spin state of the central iron atom is explored in detail. The correct description of the spin state is found to be crucial for achieving agreement between the optical spectra in simulation and experiment.

METHODS

Experiment. Tribological experiments were performed using an oscillating cylinder-on-disk sliding geometry (SRV-III, Optimol Instruments) with constant parameters (50 N normal load, 50 Hz frequency, 90 °C temperature, 1 mm amplitude). At the beginning, there is a line contact with an initial contact pressure of 130 MPa, which decreases during the tribological test due to wear.[1−3] The cylinder is inclined by 10° to the sliding direction. For the tribological tests, standardized 100Cr6 specimens (steel 1.3505) were used with a hardness of 62 HRC (Rockwell C hardness).[1−3] The disk has a roughness

Received: January 29, 2013
Revised: March 21, 2013
Published: March 27, 2013

of R_a = 0.07 μm and R_z = 0.60 μm, and the cylinder has R_a = 0.06 μm and R_z = 0.46 μm.[1−3]

For FT-IR measurements, a BioRad Excalibur FTS 3000 spectrometer was used. The different fluids were measured between two NaCl windows with a resolution of 4 cm^{-1}. The UV−vis spectra were measured between 800 and 300 nm using quartz cuvettes with a Cary Bio 50 spectrometer (Co. Varian). Acetonitrile with a molar concentration of 10^{-4} mol/L was used to dissolve the DKs for the UV−vis measurement.

Simulation. The density functional theory (DFT) calculations were performed with the grid projector augmented wave (GPAW) method.[6,7] A grid spacing of h = 0.2 Å was used for the representation of the smooth wave functions and was checked for convergence. The simulation box contained at least 4.0 Å of vacuum around the molecules, and zero boundary conditions were applied outside of the box. The exchange−correlation energy was approximated in the generalized gradient approximation (GGA) as devised by Perdew, Burke, and Ernzerhof (PBE)[8] and cross-checked with the meta-GGA functional of Tao et al. (TPSS)[9] in a non-self-consistent calculation using PBE densities. In order to obtain reliable vibrational spectra, the molecules were relaxed without symmetry constraints until the forces were lower than 0.01 eV/Å. The vibrational spectra were obtained from a finite difference approximation of the dynamical matrix and the IR intensities via a finite difference approximation of the gradient of the dipole moment.[10] The correct description of the iron complexes' electronic structure and spin state made it necessary to employ the PBE+U method,[11] as detailed below.

RESULTS AND DISCUSSION

1,3-Diketone Fluids. The DKs considered in this study are a subset of the substituted 1,3-diketones that were used as lubricants in the tribological experiments.[1] These molecules are of the structure type depicted in Figure 1, where R_1 and R_3 denote different side groups. The 1,3-diketones can appear in both enol and keto tautomeric forms,[12,13] which are distinct by the position of the hydrogen atoms (see Figure 1a). It is known that the enol form is the usually preferred tautomer at ambient conditions.[12] The keto−enol ratio increases at high temperature, large solvent polarizability,[14−16] and for a short alkyl group.[12,17]

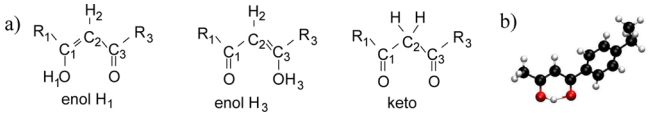

Figure 1. (a) The labeling scheme for the molecules considered in this study. Note that the subscripts are labels for the atoms only and do not denote the number of atoms. (b) The enol H_1 form of the 1,3-diketone MF-02/01; C: black, O: red, and H: white.

One of the simplest substances that falls into this class of molecules is acetylacetone (ACAC, 2,4-pentanedione[18]), where R_1 = R_3 = CH_3. This molecule has been studied broadly in the literature[13−16,19] and serves as a reference system here. We will concentrate on the smallest DKs used in the tribological studies[1] for computational reasons. These are MF-02/01, where R_1 = CH_3 and R_3 = PhC_2H_5, and MF-02/06, where R_1 = C_6H_{13} and R_3 = PhC_2H_5. Ph denotes a phenyl ring, and we have adopted the nomenclature used in ref 2 for these molecules. Note that in refs 1 and 3, the name 07/10 was used for MF-02/06.

The energetics of the tautomeric forms of the molecules considered is listed in Table 1, and pictures of the relaxed structures can be found in the Supporting Information (SI). For ACAC, we find the keto form to be 0.43 eV [0.34 eV] higher in energy in PBE [TPSS]. This result is in fair agreement with the literature, where the reported keto−enol energy difference ranges between 0.14 and 0.39 eV depending on the functional and basis set used.[14,15,17,20] It overestimates the experimental energy difference of 0.1−0.2 eV.[21−24] The dipole moment |μ| of the enol form is found to be clearly larger than that of the keto form. This is also in agreement with previous reports where dipole moments of 3.0−3.15 and 1.5−1.65 D were reported[15] for enol and keto tautomers, respectively.

Table 1. Energy Relative to the Lowest Tautomer E in eV (1 eV = 96.485 kJ/mol =23.061 kcal/mol) and the Dipole Moment |μ| (1 D = 3.33564 × 10^{-30} Cm)

MF-[m,n]	form	E PBE [eV]	E TPSS [eV]	|μ| [D]
ACAC	enol	0.0	0.0	3.22
	keto	0.43	0.34	0.93
MF-02/01	enol H_1	0.0	0.0	3.79
	enol H_3	0.01	0.02	4.15
	keto	0.36	0.28	2.04
MF-02/06	enol H_1	0.05	0.05	3.47
	enol H_3	0.0	0.0	3.90
	keto	0.36	0.29	1.74

There are two possible enol forms due to the asymmetry in R_1 and R_3 in the DKs MF-02/01 and MF-02/06. These are labeled according to which oxygen atom they are connected to (c.f. Figure 1) and are found to be practically isoenergetic. The keto−enol energetic difference of the DKs is very comparable to that of ACAC. Their dipole moments are slightly larger than that in ACAC, and the enol's |μ| roughly doubles the |μ| of the keto form. While there is nearly no difference energetically, the dipole moment does depend on the position of the hydrogen atom in the two enol forms, which shows the sensitivity of this quantity on the exact configuration of the atoms.

Experimentally, ACAC[14,16,19] and the DKs are best characterized by their IR spectra. We therefore analyze the main IR transitions in the simulation and use the knowledge gained to interpret the experimental spectra in the following. The simulated IR spectra of ACAC and the DKs are shown in Figure 2a−c. The main transitions are listed in the SI explicitly, where a detailed comparison to the ACAC IR spectra from the literature is included also.

We will just discuss the most important features here. The enol form of ACAC has one main peak at 1634 cm^{-1} that can be assigned to an in-plane bending mode of the OH bond. This frequency is in good agreement with the literature, where the reported experimental frequencies are in the range of 1615−1638 cm^{-1} (see the SI). Generally, the assignment of a vibrational mode to a limited number of atoms is not unambiguous in larger molecules as a single mode can have various contributions. In particular, this mode has also contributions from in-plane C═C and C═O stretching vibrations that lead to different assignments in the literature.[14,19] The bending mode of the hydrogen H_2 (see Figure 1 for the labeling) is much weaker and found at 1474 cm^{-1}, with experimental values of 1424−1462 cm^{-1}. The keto form shows

dx.doi.org/10.1021/jp400980y | J. Phys. Chem. A 2013, 117, 3369−3376

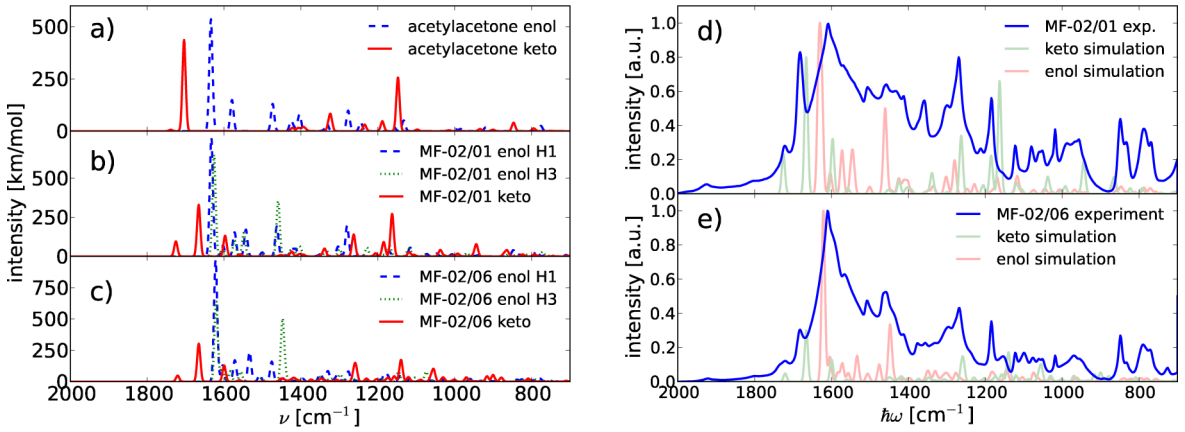

Figure 2. Simulated vibrational spectra for the different tautomers of (a) ACAC, (b) MF-02/01, and (c) MF-02/06. The simulated spectra are folded by Gaussians of 4 cm^{-1} width. Experimental IR spectra of the 1,3 diketone fluids (d) MF-02/01 and (e) MF-02/06. The simulated spectra are overlaid for better comparison in (d) and (e).

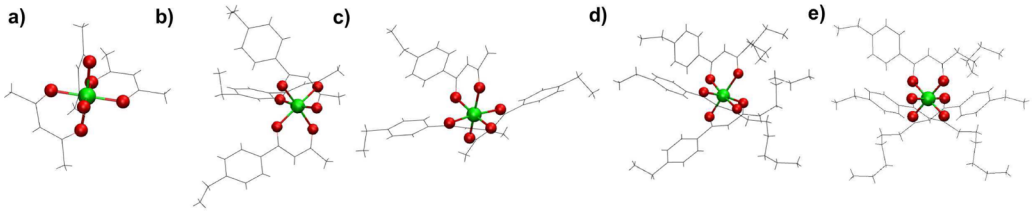

Figure 3. Relaxed structures of (a) $Fe(ACAC)_3$, $Fe(MF\text{-}02/01)_3$ in the (b) xxx and (c) xx-x configurations, and $Fe(MF\text{-}02/06)_3$ in the (d) xxx and (e) xx-x configurations (see the text). Iron (green) and oxygen atoms (red) are highlighted.

a strong C═O stretch peak at 1704 cm^{-1} (1705−1715 cm^{-1} in the experiment) and a weaker in-plane stretch mode of the C_1−C_2−C_3 backbone at 1148 cm^{-1} (1176−1179 cm^{-1} in the experiment). In conclusion, we obtain good agreement with the experiment and hence are able to clearly assign the strongest IR transitions to the tautomeric forms of ACAC.

The IR spectra of the DKs in Figure 2b,c have many similarities to the spectrum of ACAC. The strongest peak of the two enol forms is still the OH bending mode at 1633 and 1622 cm^{-1} for MF-02/01 and MF-02/06, respectively. This mode increases in intensity with increasing molecular mass. The H_2 bending mode of the enol form is found at 1463 and 1476 cm^{-1} for MF-02/01 and MF-02/06, respectively. The keto form shows two peaks related to C═O stretch vibrations, a stronger one at 1666 cm^{-1} for both DKs and a weaker one at 1163 and 1140 cm^{-1} for MF-02/01 and MF-02/06, respectively.

We now turn to the experimental IR spectrum of the DKs shown in Figure 2d,e. A very strong transition at 1609 cm^{-1} can be identified and is a clear signature of the presence of the enol form when compared to Figure 2b,c. The transitions at 1681, 1268, and 1184 cm^{-1} indicate the substantial presence of the keto form in the experiment also. Using the relative heights of enol and keto peaks suggests a larger proportion of the keto form in the liquid of MF-02/01 than that in the liquid of MF-02/06.

This dependence of the keto−enol ratio on the size of the alkyl chain R_1 cannot be explained by the gas-phase energetics from Table 1, where the same energy difference is found for both DKs. The keto form should be present only in very small quantities at ambient temperature as the energetic gap is much larger than thermal energy (k_BT = 0.026 eV at 298° K). It is known from the experiment that the polarizability of a solvent can change the energetics and lower the keto energy relative to the enol energy.[15] We do not have a solvent here, but we are dealing with the pure DKs that have their own polarizability. Application of a simple estimate of the polarizability obtained for freely rotating permanent dipoles (see the SI) leads to ε = 5.68 and 4.58 for MF-02/01 and MF-02/06 at 298° K, respectively. Although MF-02/01 has a slightly smaller dipole moment than MF-02/06, it is of smaller size, and therefore, there are more dipoles present per unit volume. The larger ε of MF-02/01 suggests that this effect could lead to a stronger presence of the keto seen in the experiment.

Iron Complexes. We now discuss the properties of iron complexes with the DKs as some of us suggested in ref 1 that there is complex formation due to a tribochemical reaction with the iron surface in the tribological experiments. This proposal will be corroborated in the following by a comparison of the simulated spectra of the iron complexes with experimental results.

The simplest DK considered in this work, ACAC, is well-known to build a chelate complex with Fe^{III}.[18,25] A similar (partial) complexation reaction is known as the salicylate detection reaction with a characteristic absorbance maximum at 535 nm = 2.32 eV, giving a strong color.[4] The reaction can be imagined in a simple picture. Disregarding the ligand field effect, the iron atom gives three electrons away to reach oxidation state III. It transforms from the neutral ground state $Fe(3d^64s^2)$ to $Fe(3d^54s^0)$, that is, to a half-filled 3d shell that should be exceptionally stable according to Hund's rules. Due to complexation, the three electrons are absorbed by three 1,3-diketone ligand radicals that are octahedrally coordinated to the central metal atom.[5] Accordingly, an experimentally crystallized Fe^{III} 1,3-diketone complex was found to be neutral.[26]

It is well-known, however, that Fe^{III} can complex into spin-crossover systems, where typically doublet and sextet spin states

dx.doi.org/10.1021/jp400980y | J. Phys. Chem. A 2013, 117, 3369−3376

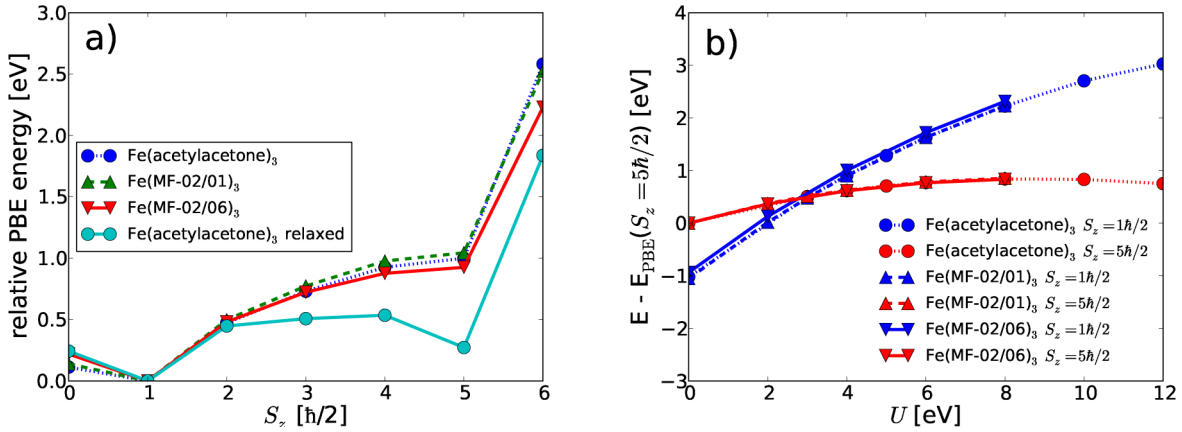

Figure 4. (a) Spin projection S_z dependence of the PBE energy. (b) Energetics using PBE+U with varying U at $S_z = 1[\hbar/2]$ and $S_z = 5[\hbar/2]$. Only xxx conformers are considered for MF-02/01 and MF-02/06.

are near in energy and their occupation can depend on temperature.[27] As an example, it was found computationally that a catecholato-Fe^{III} system in the solid state undergoes a doublet to the sextet spin-crossover with increasing temperature.[28] Fe^{III} complexes with octahedral coordination, as we are dealing with here, are typically found in the high-spin (sextet) ground state. Examples are Fe^{III}(cyclooctadiene)$_3$, where cyclooctadiene is a 1,2-diketone,[29] and Fe^{III} porphyrin difluoride.[30]

We consider the iron complexes in octahedral conformation as depicted in Figure 3. Spin-unpolarized relaxation of the structures with the PBE functional did not lead to severe structural changes, that is, these structures represent stable minima in all cases. For the asymmetric ligand molecules like MF-02/01 and MF-02/06, there are two possible conformers, one where all phenyl groups point into the same direction labeled by xxx (Figure 3b and d) and another one where one of the phenyl groups points into the opposite direction, labeled by xx-x (Figure 3c and e). Due to the similar binding motif, the structural properties do not depend on the ligand type. This is exemplified by the FeO distance, which is found to be R_{FeO} = 1.92 Å for all three ligands consistently. The xxx and xx-x conformations are within 0.02 eV (within 0.03 eV in TPSS) and therefore practically isoenergetic. This is a consequence of the steric hindrance of ligand−ligand interactions due to their octahedral conformation.

Particularly optical properties, such as the UV−vis spectrum, depend directly on the electronic structure of the complexes. We therefore address the electronic structure and in particular the spin state of the complexes in the next step. We have performed spin-polarized calculations at the spin-unpolarized geometry obtained above. DFT does not allow one to restrict the total spin but only the spin projection S_z,[31] which is defined by the difference in the occupation numbers of the majority and minority spin Kohn−Sham states resulting in different majority and minority spin densities, that is S_z = 1 (in units of $\hbar/2$) denotes one more electron in the majority than in the minority spin density. The S_z dependence of the PBE energy shown in Figure 4a is very similar to that for the three ligands (only the xxx conformers of MF-02/01 and MF-02/06 are shown as the xx-x conformers do not differ). We allow for partial occupations, and therefore, also even S_z values appear. The projection $S_z = 1[\hbar/2]$ (the doublet) leads to the minimum of the PBE energy. Although in a range of 1 eV, the energy dependence is rather flat for $S_z \leq 5[\hbar/2]$, with a steep rise for larger S_z. The flatness can be interpreted as the result of different possible projections of the total spin[32,33] due to the two possible doublet and sextet states of Fe^{III}. A very similar behavior was observed for the octahedrally coordinated difluoride iron porphine complex using the PBE functional.[30]

Relaxation of the Fe(ACAC)$_3$ at fixed spin projection S_z results in practically no structure changes for the doublet state ($S_z = 1[\hbar/2]$). In contrast, it increases the Fe−O bond length of the high-spin sextet state ($S_z = 5[\hbar/2]$) considerably to 2.04 ± 0.02 Å.[34] This structural change also results in an improved energy, as shown in Figure 4a. The relaxed sextet becomes the spin configuration with the second lowest energy and represents a real minimum now.

Nevertheless, as discussed above, we expect the sextet to be lower in energy than the doublet, which is not the case here. Difficulties of the local density approximation persisting in GGAs with strongly localized orbitals are well-known. These appear in particular in transition metals and are attributed to the self-interaction errors present in these functionals.[35] These problems can be at least partially resolved by a DFT+U approach pioneered by Anisimov et al.,[11] where a Hubbard-like energy term U is added to the metal d electrons.[35] This term effectively favors integer occupations of the d orbitals and therefore prefers their localization.[36] Both B3LYB+U and GGA +U were found to correctly describe the spin ordering in Fe^{III} complexes.[30,37−39]

We use a particular formulation, where only an effective Hubbard U parameter appears,[7,36] a method that was applied to iron complexes before.[30,37] While most approaches use U as a free parameter, as we will also do in the following, it can also be obtained by a self-consistent approach using unrestricted Hartree−Fock theory.[40] Mosey et al. reported a self-consistent value for iron oxide of U = 3.7−4.3 eV depending on the oxidation state.[40] In agreement with this result, U = 4 eV was proposed for iron oxides by Wang et al.[41]

Figure 4b shows the relative energy of the doublet and the sextet depending on U in the spin-paired relaxed geometries. The result is remarkably similar for all of the ligands considered. The clear preference of the doublet by PBE of nearly 1 eV diminishes with increasing U. At around U = 3 eV, the spin states are of equal energy, and the $S_z = 5[\hbar/2]$ state becomes the ground state for larger U. A very similar behavior was found for the heme Fe^{II} complex,[37] where the value of U = 4 eV was recommended.

dx.doi.org/10.1021/jp400980y | J. Phys. Chem. A 2013, 117, 3369−3376

Because of the clear preference of the sextet state for $U > 3$ eV seen in Figure 4b and the recommendations from the literature, we use $U = 4$ eV for the further analysis. As listed in Table 2, spin-polarized relaxation in the sextet ground state leads to an increase of the Fe−O distance in the complexes relative to that for the PBE spin-paired ground state. Independent of the ligand type, the bond length changes to $R_{FeO} = 2.04$ Å at $U = 4$ eV in comparison to 1.92 Å at $U = 0$. This increase in bond length is mainly a consequence of the sextet ground state. A similar effect is seen in a spin-restricted PBE relaxation in the sextet discussed above. The long bond length is in excellent agreement with the experimentally determined $R_{FeO} = 2.04$ Å in the Fe^{III} 1,2-dimethoxyethane complex,[29] giving a strong indication that we have found the correct structure and spin state. The comparison of IR and optical spectra with experiment will further validate these findings in the following.

Table 2. Structural and Electronic Properties of the Complexes[a]

	R_{FeO} [Å] $U = 0$ eV	R_{FeO} [Å] $U = 4$ eV	gap [eV] $U = 4$ eV
$Fe(ACAC)_3$	1.92	2.04	3.30 (2.35)
$Fe(MF\text{-}02/01)_3$ xxx	1.92	2.04	2.97 (2.32)
$Fe(MF\text{-}02/01)_3$ xx-x	1.93	2.04	2.92 (2.30)
$Fe(MF\text{-}02/06)_3$ xxx	1.92	2.03	2.83 (2.14)
$Fe(MF\text{-}02/06)_3$ xx-x	1.92	2.03	2.83 (2.14)

[a] $U = 0$ values are for the spin-paired and $U = 4$ eV values for the $S_z = 5[\hbar/2]$ state. The mean value R_{FeO} of the six iron−oxygen distances is given (the standard deviation is ≤0.01 Å). The gap is defined as the energy difference between the HOMO and LUMO of each spin separately, with the minority spin gap in parentheses.

Figure 5a−c shows the calculated vibrational spectra of the iron complexes (the main vibrational lines are given in the SI). The IR spectrum of $Fe(ACAC)_3$ consists of two strong lines at 1513 and 1563 cm^{-1}. The higher-energy vibration consists of two degenerate vibrations that can be assigned to C═O stretch vibrations, while the lower one is an in-plane vibration of the H_2 atom. A similar concentration of the vibrational lines is seen in the IR spectra of the complexes with MF-02/01 and MF-02/06 also. The two degenerate C═O stretch vibrations can be found at around 1540 cm^{-1} (see the SI for the explicit numbers) but lose intensity when the ligand gets larger. The in-plane vibration of the H_2 atom hybridizes more and more with other vibrations (e.g., gets mixed with contributions from the phenyl rings) with increasing ligand size and becomes the dominating feature in $Fe(MF\text{-}02/06)_3$. There is nearly no difference between the spectra of the xxx and the xx-x configurations.

The splitting and shifting of the main vibrational intensity to the region around 1550 cm^{-1} is also seen in the experimental IR spectra shown in Figure 5c, where the spectra of MF-02/06 and the complex $Fe(MF\text{-}02/06)_3$ are overlaid to improve the direct comparison (note that the similarity of the vibrational spectra between MF-02/06 and the corresponding complex, in particular for vibrations lower than 1300 cm^{-1}, indicates the presence of pure DK in the experimental $Fe(MF\text{-}02/06)_3$ complex). A similar effect of shifting and splitting in the vibrational lines has been found experimentally for the spectra of copper(II) diketonate complexes.[42] The IR spectrum of MF-02/06 after 20 h of tribological experiment is depicted in Figure 5d. It clearly shows the presence of the complex within the DK, strongly supporting the assumption of complex formation in the tribological experiment.[1]

We now want to further discuss the electronic structure of the complexes. In contrast to the energy calculations, the electronic structure is less sensitive to the grid spacing (see the SI for the similarity of optical spectra obtained with grids using different grid spacings). Therefore, we have used the computationally cheaper grid spacing $h = 0.25$ Å for the representation of the smooth wave functions in analysis of the electronic structure and the electronic excited-state properties. As listed in Table 2, the complexes at $S_z = 5[\hbar/2]$ possess HOMO−LUMO gaps of more than 2 eV in both spin manifolds (HOMO = highest occupied molecular orbital; LUMO = lowest unoccupied molecular orbital). The gaps are always smaller for the minority spin manifold and decrease with increasing ligand size.

In order to obtain a better understanding of the effect of U, we compare the electronic structure for $U = 0$ and 4 eV in

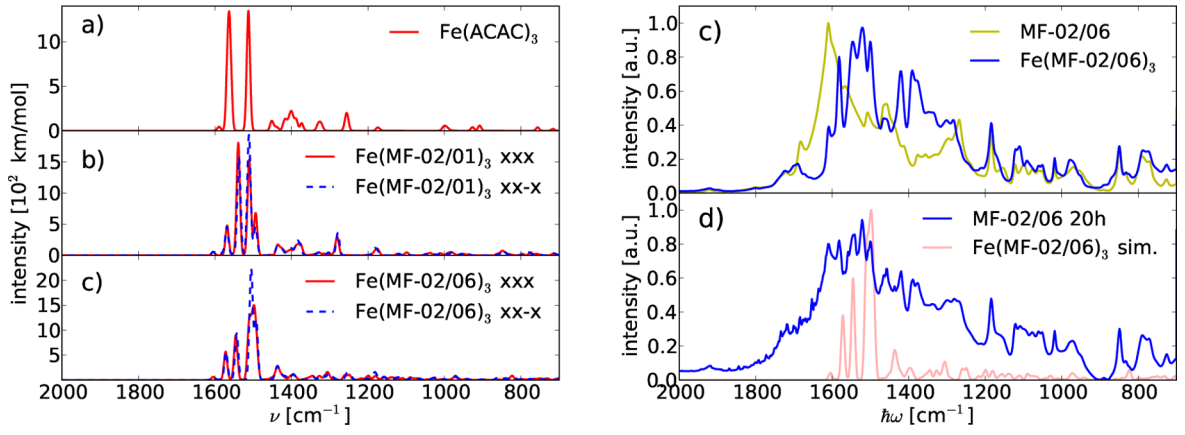

Figure 5. Simulated (a−c) and measured (d,e) vibrational spectra for the iron complexes. The simulated vibrational spectra of (a) ACAC, (b) MF-02/01, and (c) MF-02/06 are folded by Gaussians of 4 cm^{-1} width. The experimental spectra were obtained from (c) the pure MF-02/06 and pure $Fe(MF\text{-}02/06)_3$ complex and (d) MF-02/06 after a 20 h tribological experiment. The simulated spectrum of MF-02/06 is overlaid for better comparison in (d).

dx.doi.org/10.1021/jp400980y | J. Phys. Chem. A 2013, 117, 3369−3376

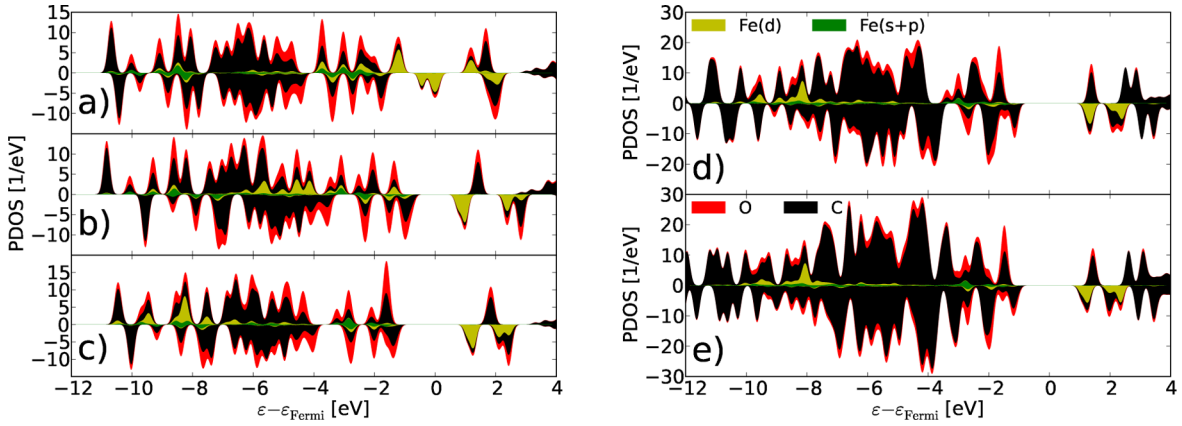

Figure 6. Projected density of states (PDOS) of the complexes in the relaxed configurations of each spin state and functional. $Fe(ACAC)_3$ in (a) the doublet with PBE, (b) the sextet with PBE, and (c) the sextet with PBE+*U*, *U* = 4 eV. (d) $Fe(MF\text{-}02/01)_3$ and (e) $Fe(MF\text{-}02/06)_3$ are in the xxx configuration with PBE+*U*, *U* = 4 eV. The majority and minority spin PDOS are plotted as positive and negative numbers respectively. The color codes are given in (d) and (e).

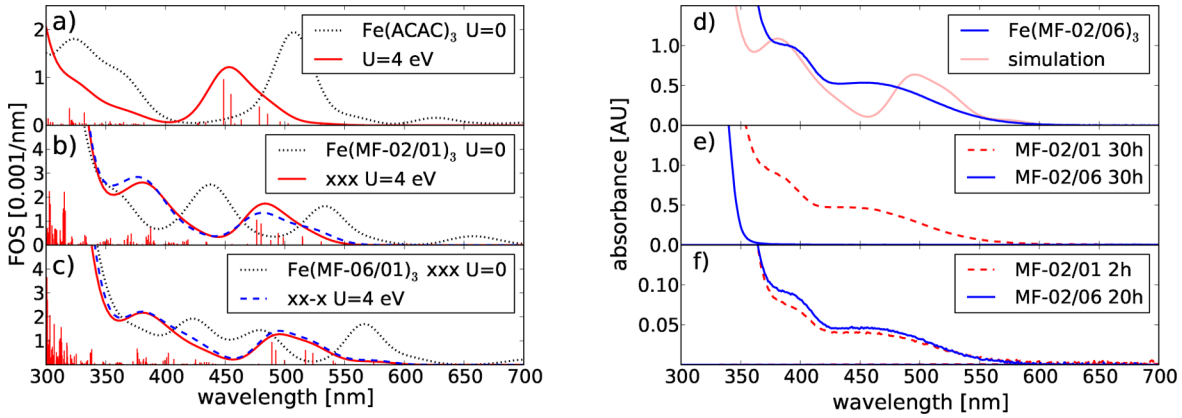

Figure 7. Simulated optical spectra for the iron complexes with (a) ACAC, (b) MF-02/01, and (c) MF-02/06. The folded oscillator strength (FOS) was obtained by folding with Gaussians of 15 nm width. Experimental UV−vis absorbance spectra (d) of the pure $Fe(MF\text{-}02/06)_3$ complex, (e) of MF-02/01 and MF-02/06 after 30 h of reaction (see text), and (f) of MF-02/01 and MF-02/06 after the tribological experiment. The simulated spectrum for *U* = 4 eV of (c) is overlaid for better comparison in (d).

Figure 6, which shows the density of states around the Fermi energy projected on the elements (PDOS). The PBE (*U* = 0) doublet PDOS of $Fe(ACAC)_3$ in Figure 6a has a clear HOMO−LUMO gap for the majority spin, but the minority spin has two half-filled, nearly degenerated Fe(d) orbitals at the Fermi energy. The PBE (*U* = 0) sextet of $Fe(ACAC)_3$ in Figure 6b opens a gap also for the minority spin manifold and lets the LUMO orbitals be built of Fe(d) orbitals. The occupied Fe(d) orbitals are distributed over a large energy range including the HOMO. Applying *U* = 4 localizes the Fe(d) orbitals and therefore reduces their energy splitting, as shown in Figure 6c. The LUMO orbitals are still purely Fe(d), but the occupied Fe(d) are very deep, around −9 eV relative to the Fermi level. The HOMO orbitals of both spin manifolds are now located on oxygen and carbon atoms. While the overall PDOS depends on the ligand type, the Fe PDOS is rather independent, as can be seen in the comparison of Figure 6c−e.

Finally, we report the optical spectra of the complexes formed by the DKs in Figure 7. The spectra are also contrasted to the corresponding spectra using the PBE ground state (*U* = 0) in the PBE relaxed geometry at S_z = 5. The spectra for *U* = 0 and 4 eV are clearly different, both in position and number of maxima. The spectra at *U* = 4 eV of MF-02/01 and MF-02/06 show two maxima at ∼490 and ∼370 nm. Although the HOMO−LUMO gaps are different for MF-02/01 and MF-02/06 and the peaks consist of several transitions, the total spectra are very similar. The spectra are also in excellent agreement with the experimental UV−vis spectra depicted in Figure 7d−f. Figure 7d shows the spectrum of the pure complex of MF-02/06 as obtained from Nematel GmbH. The spectrum shows two maxima at nearly the same frequencies as those found in the simulation. A controlled reaction of the MFs to produce the complex results in a similar optical spectrum as seen in Figure 7e. Here, pure iron powder (diameter ≈ 150 μm) was mixed with three times the molar quantity of MF-02/01 and MF-02/06. The mixture was heated to 90 °C for 30 h, and the UV−vis measurement was performed after cooling to room temperature. The spectra obtained clearly reveal the different reactivities of the two MFs. While the smaller MF-02/01 shows the signatures of the complex, this is not the case for MF-02/06. The optical signal of the complex is clearly visible in the spectra recorded after 2 and 30 h of tribological experiment for MF-02/01 and MF-02/06, respectively, in Figure 7f. In agreement with the reactivity study, the smaller MF-02/01 needs a shorter tribological treatment to show the complex.

dx.doi.org/10.1021/jp400980y | *J. Phys. Chem. A* 2013, 117, 3369−3376

CONCLUSIONS

In conclusion, we have analyzed the energetics of the 1,3-diketone fluids used in the tribological experiments and simulated the IR spectra of the different tautomers. We obtained good agreement with the experimentally measured spectra and can assign vibrational lines to the tautomers, proving their presence in the experimental samples. The dependence of the keto−enol ratio on the ligand type can be rationalized by a simple model for the polarizability of the 1,3-diketone fluids.

In order to check the assumption of complex formation, we also studied the geometric and electronic structure of Fe(III) complexes. We found that the use of PBE+U with an effective U = 4 eV provides the expected sextet spin state. The spin state was shown to influence the structure of the complex in that the high spin state increases the iron−oxygen distance markedly. Within the PBE+U approach, the simulated IR as well as optical spectra are in very good agreement with those from the experiment. We therefore clearly can approve the formation of Fe(III) complexes during the tribological experiment.

From the computational perspective, we have proved that the inclusion of U is necessary but also sufficient to obtain meaningful infrared and optical spectra that can be directly compared to the experiment. In particular, the optical spectra are strongly influenced by U and change dramatically when U is changed. We found a good match to the experimental UV−vis spectra for U = 4 eV, while the correlation between the PBE optical spectrum and the experiment is hardly possible.

ASSOCIATED CONTENT

Supporting Information

Pictures of the different tautomers of the 1,3-diketones, their vibrational frequencies in comparison to the literature, and the estimate of the polarizability. The main vibrations of the Fe(III)(1,3-diketone)$_3$ complexes are listed, and the convergence of the optical spectrum with grid spacing is shown. This material is available free of charge via the Internet at http://pubs.acs.org.

AUTHOR INFORMATION

Corresponding Author

*E-mail: Michael.Walter@fmf.uni-freiburg.de.

Notes

The authors declare no competing financial interest.

ACKNOWLEDGMENTS

M.W. thanks Alexander Held for help with the estimate of the polarizabilities using the rigid dipole model. M.W., T.A., and K.L. acknowledge funding from the Deutsche Forschungsgemeinschaft (Grant No. BA 60026). M.W. gratefully thanks FZ Jülich, RZ Karlsruhe, and the bwGRiD project[43] for the computational resources.

REFERENCES

(1) Amann, T.; Kailer, A. Analysis of the Ultralow Friction Behavior of a Mesogenic Fluid in a Reciprocating Line Contact. *Wear* **2011**, *271*, 1701−1706.

(2) Amann, T.; Kailer, A. Relationship Between Ultralow Friction of Mesogenic-Like Fluids and Their Lateral Chain Length. *Tribol. Lett.* **2011**, *41*, 121−129.

(3) Amann, T.; Kailer, A. Ultralow Friction of Mesogenic Fluid Mixtures in Tribological Reciprocating Systems. *Tribol. Lett.* **2010**, *37*, 343−352.

(4) Mitchell-Koch, J. T.; Reid, K. R.; Meyerhoff, M. E. Salicylate Detection by Complexation with Iron(III) and Optical Absorbance Spectroscopy. *J. Chem. Educ.* **2008**, *85*, 1658.

(5) Giroud-Godquin, A. M. My 20 Years of Research in the Chemistry of Metal Containing Liquid Crystals. *Coord. Chem. Rev.* **1998**, *178−180*, 1485−1499.

(6) Mortensen, J. J.; Hansen, L. B.; Jacobsen, K. W. Real-Space Grid Implementation of the Projector Augmented Wave Method. *Phys. Rev. B* **2005**, *71*, 035109.

(7) Enkovaara, J.; et al. Electronic Structure Calculations with GPAW: A Real-Space Implementation of the Projector Augmented-Wave Method. *J. Phys.: Cond. Mat.* **2010**, *22*, 253202.

(8) Perdew, J. P.; Burke, K.; Ernzerhof, M. Generalized Gradient Approximation Made Simple. *Phys. Rev. Lett.* **1996**, *77*, 3865−3868.

(9) Tao, J.; Perdew, J. P.; Staroverov, V. N.; Scuseria, G. E. Climbing the Density Functional Ladder: Nonempirical Meta-Generalized Gradient Approximation Designed for Molecules and Solids. *Phys. Rev. Lett.* **2003**, *91*, 146401.

(10) Porezag, D.; Pederson, M. R. Infrared Intensities and Raman-Scattering Activities within Density-Functional Theory. *Phys. Rev. B* **1996**, *54*, 7830−7836.

(11) Anisimov, V. I.; Solovyev, I. V.; Korotin, M. A.; Czyżyk, M. T.; Sawatzky, G. A. Density-functional Theory and NiO Photoemission Spectra. *Phys. Rev. B* **1993**, *48*, 16929−16934.

(12) Bassetti, M.; Cerichelli, G.; Floris, B. Substituent Effects in Keto−Enol Tautomerism. Part 3.1 Influence of Substitution on the Equilibrium Composition of of β-Dicarbonyl Compounds. *Tetrahedron* **1988**, *44*, 2997−3004.

(13) Pocker, Y.; Spyridis, G. T. Modulation of Tautomeric Equilibria by Ionic Clusters. Acetylacetone in Solutions of Lithium Perchlorate-Diethyl Ether. *J. Am. Chem. Soc.* **2002**, *124*, 10373−10380.

(14) Nagashima, N.; Kudoh, S.; Takayanagi, M.; Nakata, M. UV-Induced Photoisomerization of Acetylacetone and Identification of Less-Stable Isomers by Low-Temperature Matrix-Isolation Infrared Spectroscopy and Density Functional Theory Calculation. *J. Phys. Chem. A* **2001**, *105*, 10832−10838.

(15) Schlund, S.; Janke, E. M. B.; Weisz, K.; Engels, B. Predicting the Tautomeric Equilibrium of Acetylacetone in Solution. I. The Right Answer for the Wrong Reason? *J. Comput. Chem.* **2010**, *31*, 665−670.

(16) Karabulut, S.; Namli, H. An FT-IR and DFT Based New Approach for the Detection of Tautomer Proportions in Solution. *J. Mol. Struct.* **2012**, *1024*, 151−155.

(17) Cabral do Couto, P.; Costa Cabral, B. J.; Martinho Simoes, J. The Enthalpy of Formation of the Pentane-2,4-dionate Radical: A Complete Basis Set Approach. *Chem. Phys. Lett.* **2006**, *419*, 486−491.

(18) Charles, R. G.; Barnartt, S. Reaction of Acetylacetone with Metallic Iron in the Presence of Oxygen. *J. Phys. Chem.* **1958**, *62*, 315−318.

(19) Lozada-Garcia, R. R.; Ceponkus, J.; Chin, W.; Chevalier, M.; Crépin, C. Acetylacetone in Hydrogen Solids: IR Signatures of the Enol and Keto Tautomers and UV Induced Tautomerization. *Chem. Phys. Lett.* **2011**, *504*, 142−147.

(20) Chen, X.-B.; Fang, W.-H.; Phillips, D. L. Theoretical Studies of the Photochemical Dynamics of Acetylacetone: Isomerzation, Dissociation, and Dehydration Reactions. *J. Phys. Chem. A* **2006**, *110*, 4434−4441.

(21) Nakanishi, H.; Morita, H.; Nagakura, S. Electronic Structures and Spectra of the Keto and Enol Forms of Acetylacetone. *Bull. Chem. Soc. Jpn.* **1977**, *50*, 2255−2261.

(22) Hacking, J.; Pilcher, G. Enthalpy of Combustion of Pentane-2,4-dione. *J. Chem. Thermodyn.* **1979**, *11*, 1015−1017.

(23) Folkendt, M. M.; Weiss-Lopez, B. E.; Chauvel, J. P.; True, N. S. Gas-Phase Proton NMR Studies of Keto−Enol Tautomerism of Acetylacetone, Methyl Acetoacetate, and Ethyl Acetoacetate. *J. Phys. Chem.* **1985**, *89*, 3347−3352.

(24) Hush, N. S.; Livett, M. K.; Peel, J. B.; Willett, G. D. Variable-Temperature Ultraviolet Photoelectron-Spectroscopy of the Keto−Enol Tautomers of Pentane-2,4-dione. *Aust. J. Chem.* **1987**, *40*, 599−609.

(25) Brito, H.; Brito, V.; Springer, J. Chelatbildung von 5-Methyl-5-hexen-2,4-dion/Styrol- Copolymeren in Lösung und an Metallischen Oberflächen. *Makromol. Chem.* **1977**, *178*, 2507−2514.
(26) Saalfrank, R. W.; Hörner, B.; Stalke, D.; Salbeck, J. The First Neutral Adamantanoid Iron(III)-Chelate Complex: Spontaneous Formation, Structure, and Electrochemistry. *Angew. Chem., Int. Ed.* **1993**, *32*, 1179−1182.
(27) Nihei, M.; Shiga, T.; Maeda, Y.; Oshio, H. Spin Crossover Iron(III) Complexes. *Coord. Chem. Rev.* **2007**, *251*, 2606−2621.
(28) Simaan, A. J.; Boillot, M.-L.; Carrasco, R.; Cano, J.; Girerd, J.-J.; Mattioli, T. A.; Ensling, J.; Spiering, H.; Gütlich, P. Electronic, Vibrational, and Structural Properties of a Spin-Crossover Catecholato-Iron System in the Solid State: Theoretical Study of the Electronic Nature of the Doublet and Sextet States. *Chem.—Eur. J.* **2005**, *11*, 1779−1793.
(29) Spikes, G. H.; Bill, E.; Weyhermüller, T.; Wieghardt, K. Transition-Metal Complexes with Singly Reduced 1,2-Diketone Radical Ligands. *Angew. Chem., Int. Ed.* **2008**, *47*, 2973−2977.
(30) Panchmatia, P. M.; Ali, M. E.; Sanyal, B.; Oppeneer, P. M. Halide Ligated Iron Porphines: A DFT+U and UB3LYP Study. *J. Phys. Chem. A* **2010**, *114*, 13381−13387.
(31) Wang, J.; Becke, A. D.; Vedene, H.; Smith, J. Evaluation of $\langle S^2 \rangle$ in Restricted, Unrestricted Hartree−Fock, and Density Functional Based Theories. *J. Chem. Phys.* **1995**, *102*, 3477−3480.
(32) Moseler, M.; Häkkinen, H.; Barnett, R. N.; Landman, U. Structure and Magnetism of Neutral and Anionic Palladium Clusters. *Phys. Rev. Lett.* **2001**, *86*, 2545−2548.
(33) Borgh, M.; Toreblad, M.; Koskinen, M.; Manninen, M.; Åberg, S.; Reimann, S. M. Correlation and Spin Polarization in Quantum Dots: Local Spin Density Functional Theory Revisited. *Int. J. Quantum Chem.* **2005**, *105*, 817−825.
(34) The "error" given is the standard deviation as obtained from the six Fe−O bonds.
(35) Cramer, C. J.; Truhlar, D. G. Density Functional Theory for Transition Metals and Transition Metal Chemistry. *Phys. Chem. Chem. Phys.* **2009**, *11*, 10757−10816.
(36) Dudarev, S. L.; Botton, G. A.; Savrasov, S. Y.; Humphreys, C. J.; Sutton, A. P. Electron-Energy-Loss Spectra and the Structural Stability of Nickel Oxide: An LSDA+U Study. *Phys. Rev. B* **1998**, *57*, 1505−1509.
(37) Scherlis, D. A.; Cococcioni, M.; Sit, P.; Marzari, N. Simulation of Heme Using DFT + U: A Step toward Accurate Spin-State Energetics. *J. Phys. Chem. B* **2007**, *111*, 7384−7391.
(38) Sarkar, S.; Tarafder, K.; Oppeneer, P. M.; Saha-Dasgupt, T. Spin-Crossover in Cyanide-Based Bimetallic Coordination Polymers — Insight from First-Principles Calculations. *J. Mater. Chem.* **2011**, *21*, 13832.
(39) Ali, M. E.; Sanyal, B.; Oppeneer, P. M. Electronic Structure, Spin-States, and Spin-Crossover Reaction of Heme-Related Fe-Porphyrins: A Theoretical Perspective. *J. Phys. Chem. B* **2012**, *116*, 5849−5859.
(40) Mosey, N. J.; Liao, P.; Carter, E. A. Rotationally Invariant Ab Initio Evaluation of Coulomb and Exchange Parameters for DFT+ U Calculations. *J. Chem. Phys.* **2008**, *129*, 014103.
(41) Wang, L.; Maxisch, T.; Ceder, G. Oxidation Energies of Transition Metal Oxides within the GGA+ U Framework. *Phys. Rev. B* **2006**, *73*, 195107.
(42) David, L.; Craciun, C.; Cozar, O.; Chis, V.; Agut, C.; Rusu, D.; Rusu, M. Spectroscopic Studies of Some Oxygen-Bonded Copper(II) *β*-Diketonate Complexes. *J. Mol. Struct.* **2001**, *563*−*564*, 573−578.
(43) *bwGRiD*, member of the German D-Grid initiative, funded by the Ministry for Education and Research and the Ministry for Science, Research and Arts Baden-Wuerttemberg. http://www.bw-grid.de (2013).